Hindawi Publishing Corporation
Journal of Nanomaterials
Volume 2012, Article ID 427453, 10 pages
doi:10.1155/2012/427453

Research Article

Relationship between Synthesis Conditions and Photocatalytic Activity of Nanocrystalline TiO_2

Yosep Han,[1] Hyung-Seok Kim,[2] and Hyunjung Kim[3]

[1] *Department of Natural Resource and Environmental Engineering, Hanyang University, 17 Heangang-Dong, Seongdong-gu, Seoul 133-791, Republic of Korea*
[2] *Mineral Resources Research Division, Korea Institute of Geoscience and Mineral Resources, Daejeon 305-350, Republic of Korea*
[3] *Department of Mineral Resources and Energy Engineering, Chonbuk National University, 664-14 Duckjin-Dong, Duckjin-gu, Jeonju, Jeonbuk 561-756, Republic of Korea*

Correspondence should be addressed to Hyunjung Kim, kshjkim@jbnu.ac.kr

Received 25 March 2012; Revised 3 June 2012; Accepted 3 June 2012

Academic Editor: Jiaguo Yu

The degradation efficiency of methylene blue by TiO_2 nanoparticles, which were synthesized under different synthesis conditions (i.e., molar ratio of water and titanium tetraisopropoxide (TTIP), pH, and calcination temperature) in a sol-gel process, was systematically investigated. The results showed that increasing the molar ratio of water and TTIP led to the enhanced photocatalytic activity of TiO_2 nanoparticles, which were likely attributed to the increased specific surface area of TiO_2 nanoparticles synthesized with high molar ratio. The results were supported by the relative increase in the size of interaggregated pores of the aggregated TiO_2 nanoparticles. The best photocatalytic activity of TiO_2 nanoparticles was observed at acidic synthesis conditions; however, the results were not consistent with physical properties for the crystallinity and the crystallite size of TiO_2 nanoparticles but rather explained by the presence of abundant hydroxyl groups and water molecules existing on the surface of TiO_2 under acidic synthesis environments. Furthermore, methylene blue degradation experiments revealed that the photocatalytic activity of TiO_2 nanoparticles was maximized at the calcination temperature of 700°C. The trend was likely due to the combined effect of the anatase crystallinity which showed the highest value at 700°C and the crystallite size/specific surface area which did not excessively increase up to 700°C.

1. Introduction

TiO_2 is utilized in different environmental applications, such as gas sensors [1, 2] and photocatalytic degradation of various contaminants in waste-air and/or wastewater treatment [3–6]. TiO_2 usually has two crystalline phases, anatase (E_g = 3.2 eV) and rutile (E_g = 3.0 eV), and the anatase phase frequently exhibits higher photocatalytic activity than the rutile phase [7–10]. The most popular commercial TiO_2 named by Degussa P25, containing around 70% anatase and 30% rutile, is known to possess excellent photocatalytic activity [7, 11]. The high activity of Degussa P25 was mainly attributed to the mixed phase composition and the high anatase crystallinity, which would favor photo-induced charge separation as well as large specific surface area.

In addition to the phase composition, the specific surface area and anatase crystallinity are important factors influencing the photocatalytic performance of TiO_2. Photocatalytic reactions using TiO_2 particles degrade pollutants by interaction with contaminants on the surfaces of the particles. Therefore, as the specific surface area of the particles increases, the contact area with contaminants increases and consequently the degradation efficiency increases. Also, increasing anatase crystallinity results in the decrease in the recombination rate of the electrons and holes so that the photocatalytic efficiency improves [7, 12, 13].

Generally, a sol-gel method based on the hydrolysis of titanium alkoxide is widely used to synthesize TiO_2 nanoparticles [14]. However, this method encounters some problems, such as weak anatase crystallinity and poor monodispersity. In addition, nanocrystalline TiO_2 prepared by the sol-gel method undergoes both phase transformation and crystallite size growth even at relative low temperature [15]. To apply TiO_2 particles synthesized from the sol-gel process

as photocatalytic catalysts, it is important to maintain high anatase crystallinity [16]. Previous study reported that high degree of anatase crystallinity can be achieved without high temperature calcination when TiO_2 particles were synthesized at low temperature due to fast hydrolysis and slow condensation [17]. In addition, many studies regarding the evaluation of the photocatalytic activity of TiO_2 nanoparticles have been conducted (e.g., [12, 18–20]); however, few focused on the correlation between parameters used in the synthesis process of TiO_2 nanoparticles and their photocatalytic activity [18, 21].

Therefore, this study was designed to investigate the effect of synthesis conditions (i.e., molar ratio (water: titanium tetraisopropoxide (TTIP)), pH, and calcination temperature) on physicochemical surface characteristics (e.g., specific surface area, pore volume, crystallinity, and crystallite size of synthesized TiO_2, and functional groups onto the surface of TiO_2 nanoparticles) as well as initial photocatalytic activity of TiO_2 nanoparticles for the samples synthesized under different conditions.

2. Materials and Methods

2.1. Preparation of TiO_2 Nanoparticles. The nanocrystalline TiO_2 particles were prepared via a sol-gel process using TTIP (Sigma-Aldrich, St. Louis, MO) and deionized water (Milli-Q, Millipore, Bedford, MA) as the starting materials. TTIP was dissolved in anhydrous alcohol (Sigma-Aldrich). The molar composition of the prepared solution was 1 : 30 (TTIP : alcohol). The controlled solution was then added dropwise to a known amount of deionized water. The molar ratios of deionized water and TTIP were set to 2, 5, 10, 20, and 50. In order to investigate the effect of the synthesis pH value on the phase transformation (anatase to rutile) and crystallite size, hydrochloric acid or aqueous ammonia was dropped into the mixed solution to yield gels with different pH values. The hydrolysis reaction was maintained under agitation condition at a reaction temperature of 20°C for 24 h. Under these conditions, the precipitation took place rapidly. The as-synthesized samples were recovered by centrifugation (MF80, Hanil, Seoul, Korea), rinsed with deionized water and alcohol, and dried at 80°C for 24 h. The synthesized TiO_2 nanoparticles were calcined with a heat rising rate of 3°C min^{-1} and a keeping time of 2 h. The temperature range investigated herein was 400–1000°C.

2.2. Photocatalytic Activity. A quartz glass reactor with a lamp immersed in the inner part of the reactor was used for all the photocatalytic experiments. The batch reactor was filled with 250 mL of an aqueous dispersion in which the concentrations of TiO_2 and methylene blue were 0.5 g L^{-1} and 10 mg L^{-1}, respectively. Photocatalytic activity of the synthesized TiO_2 was compared with that of P25, and the solution without TiO_2 catalysts was set as the point of comparison to consider the effect of pure degradation by the light source. In order to quantitatively compare the relative photocatalytic activity of TiO_2 samples, first-order reaction rate constant (k) for each sample was obtained from the degradation data with irradiation time [22]. Prior to the emission of UV light, the reactor containing TiO_2 particles and methylene blue was left for 30 min in a dark room to allow the adsorption/desorption equilibrium condition to be met [23]. A 120 W high pressure mercury lamp (Daesung Lamp Co., Republic of Korea) with a wavelength of 320–400 nm (a maximum emission at about 350 nm) and a light intensity of 12.0 MW cm^{-2} at 350 nm was used as UV light sources. After photocatalytic reaction, the samples were immediately centrifuged and the quantitative determination of methylene blue was performed by a UV-vis spectrophotometer (CE 3041, Cecil, UK).

2.3. Characterization of TiO_2 Nanoparticles. X-ray diffraction (XRD) studies were carried out by using an X-ray diffractometer (Bruker D8 HRXRD, Germany). X-ray diffraction patterns were recorded using CuKα radiation in the step-scan mode with a 2θ range of 10° to 80°. The scanning was performed in steps of 0.015° 2θ with an interval of 10 sec. The crystallite size and the relative amounts of the anatase and rutile phase were calculated from the (101) reflection of anatase and the (110) reflection of rutile. The crystallite size of anatase and rutile phase was calculated using the Scherrer's equation [22]:

$$t = \frac{k\lambda}{s\cos\theta}, \tag{1}$$

where t is the crystallite size, λ is the wavelength of the X-ray radiation (CuKα = 0.15406 nm, 40 kV, 40 mV), k is a constant that was set to 0.94, θ is the diffraction angle, and s is the line width at half maximum height. The weight fractions of anatase present in TiO_2 nanoparticles synthesized under various conditions were calculated using the equation given below [24]:

$$\chi = \frac{1}{1 + 1.26(I_A/I_R)}, \tag{2}$$

where χ is the weight fraction of the anatase phase, I_A is the diffraction peak intensity of the anatase (101) phase, and I_R is the diffraction peak intensity of the rutile (110) phase. Nitrogen adsorption to synthesized nanoparticles was measured using an AutoSorb-1 system from Quantachrome Instruments (Syosset, NY). The samples were evacuated prior to each measurement at 300°C in a high vacuum for 6 h. Specific surface area, pore size distributions, and pore volume were calculated from nitrogen adsorption isotherms. Specific surface area (S_{BET}) was calculated from the data obtained from partial relative pressure ranged between 0.05 and 0.25 using the Brunauer-Emmett-Teller (BET) method [25, 26]. Pore volume and pore size distributions were determined from the amount of nitrogen adsorbed at a relative pressure of 0.99 and by the Barrett-Joyner-Halenda (BJH) method [27, 28]. The morphology of prepared TiO_2 nanoparticles was determined by transmission electron microscopy (FE-TEM, JEM-2100F, JEOL, Japan). The accelerating voltage of the electron beam was 220 kV. The samples for TEM measurements were suspended in ethanol and dropped onto holey carbon films supported

Table 1: Results for the photodecomposition of methylene blue using the nanocrystalline TiO_2 powders synthesized at various conditions.

	Sample	Adsorption amount[a] ($mg\,g^{-1}$)	First-order reaction rate constant (k)[b] (h^{-1})	Decomposition ratio[c] (—)
	P25	0.80	0.536	0.460
Molar ratio[d] (—)	2	0.41	0.295	0.263
	5	1.10	0.690	0.538
	10	1.21	0.786	0.621
	20	1.68	0.846	0.640
	50	2.02	0.873	0.657
pH[e]	2.5	1.03	0.894	0.658
	4	0.92	0.864	0.641
	7	1.10	0.690	0.538
	9	0.85	0.588	0.480
	11	1.46	0.551	0.440
Temperature[f] (°C)	400	2.37	0.516	0.395
	500	1.21	0.431	0.357
	600	1.10	0.690	0.538
	700	0.98	0.871	0.614
	800	0.22	0.701	0.515
	900	0.20	0.468	0.376
	1000	0.20	0.511	0.385

[a]Amount of methylene blue adsorbed for first 30 min (refer to the adsorption zone in Figures 1, 5, and 8).
[b]Value determined by fitting the data for the photolysis zone in Figures 1, 5, and 8 to first-order reaction.
[c]Ratio between degraded and initial amounts.
[d]Other synthesis conditions are as follows: pH = 7 and calcination temperature = 600 °C.
[e]Other synthesis conditions are as follows: molar ratio = 5 and calcination temperature = 600 °C.
[f]Other synthesis conditions are as follows: molar ratio = 5 and pH = 7.

Table 2: Physicochemical properties of the TiO_2 nanoparticles synthesized with different molar ratios of water and TTIP. The TiO_2 synthesis was carried out at pH 7 and at a calcination temperature of 600°C.

Molar ratio (—)	Phase content[a]	S_{BET}[b] ($m^2\,g^{-1}$)	Pore volume[b] ($mm^3\,g^{-1}$)	Crystalline size[c] (nm)
2	(A): 100	29.6	38	18.2
5	(A): 100	38.2	69	18.0
10	(A): 100	44.0	58	19.2
20	(A): 100	51.0	92	18.5
50	(A): 82.5	63.9	110	(A): 18.5
	(R): 17.5			(R): 19.3

[a]A and R represent anatase and rutile, respectively.
[b]Value calculated from nitrogen adsorption isotherm.
[c]Value calculated using the Scherrer's equation [22].

on Cu grids for imaging. Surface functional groups were examined using a Fourier transform infrared spectrometer (FT-IR, FT/IR-4100, JASCO, Japan) in the range of 650–4000 cm^{-1}.

3. Results and Discussion

3.1. Effect of Molar Ratio of Water and TTIP on Photocatalytic Activity of TiO_2. Figure 1 and Table 1 represent the initial adsorption amount of methylene blue and the photocatalytic activity of synthesized TiO_2 according to the amount of water added during TiO_2 synthesis process. The pH of the water added was 7, and the calcination temperature was set to 600°C. The adsorption amount of methylene blue increased with increasing molar ratio, which is consistent with increasing specific surface area of TiO_2 samples with increasing molar ratio (Table 2). For the photocatalytic activity of TiO_2 samples, greater degree of degradation for methylene blue was observed for higher water concentration ranges, and particularly the enhancement of photocatalytic activity was pronounced when the molar ratio was greater than 20 (i.e., $k = 0.873$ and $0.846\,h^{-1}$ for the samples with molar ratio of 50 and 20, resp.). Moreover, except for the TiO_2 sample produced with a molar ratio of 2, all samples were found to have higher activity than P25.

Figure 2 and Table 2 show an XRD pattern of the synthesized TiO_2 prepared with different molar ratios of water and TTIP. The XRD peaks at $2\theta = 25.28$ and $2\theta = 27.40$ are known to be the characteristic peaks of anatase (101) and rutile (110) crystal phases, respectively [5]. An anatase (101) phase started to appear from the sample with a molar ratio of 2, and the phase was maintained until the

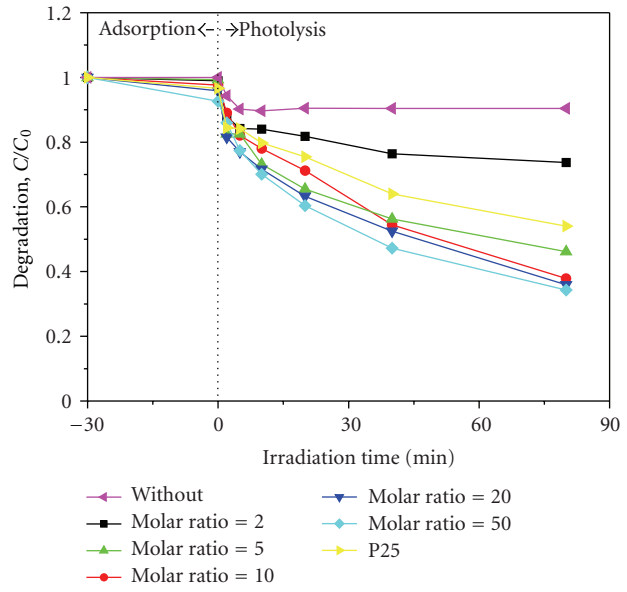

Figure 1: Photocatalytic degradation of methylene blue by TiO_2 nanoparticles synthesized with different molar ratios of water and TTIP. The TiO_2 synthesis was carried out at pH 7 and at a calcination temperature of 600°C. The results from the experiments with P25 and without TiO_2 nanoparticles were also presented for comparison purpose.

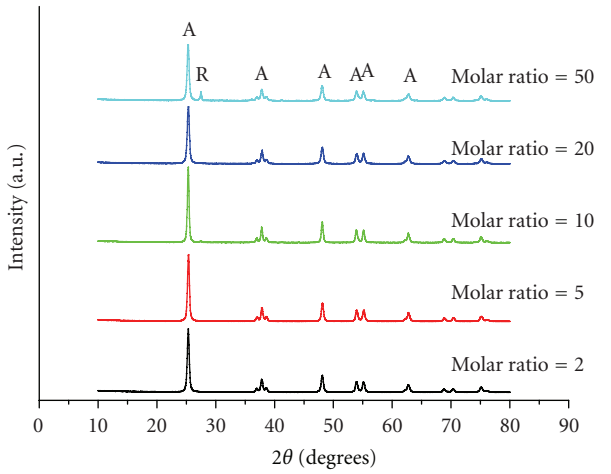

Figure 2: XRD patterns of TiO_2 nanoparticles synthesized with different molar ratios of water and TTIP. The TiO_2 synthesis was carried out at pH 7 and at a calcination temperature of 600°C. A and R represent anatase and rutile, respectively.

molar ratio was 20. The existence of the anatase phase over the broad range of molar ratio is likely due to the calcination temperature (i.e., 600°C) [15]. However, the TiO_2 samples with the molar ratio of 50 exhibited a rutile peak, indicating that phase transition from anatase to rutile started to occur at this point (Figure 2 and Table 2). This suggests that excessive water additive caused a phase transition for the synthesized TiO_2 as observed from a previous study [29]. However, regardless of the molar ratio, the crystallite size for the synthesized TiO_2 samples was consistently measured to be about 18-19 nm (Table 2), indicating that the crystallite size of the synthesized TiO_2 was not significantly affected by the water amount added.

In order to understand the effect of molar ratio of water and TTIP on the photocatalytic activity of synthesized TiO_2, physical properties (i.e., pore volume and specific surface area) of the synthesized TiO_2 particles were evaluated, and the results are presented in Table 2. The results showed that the specific surface area and pore volume increased with increasing molar ratio (i.e., increasing water amount). Particularly, for the TiO_2 sample synthesized with the largest molar ratio of 50, the specific surface area and pore volume were determined to be 63.9 $m^2 g^{-1}$ and 110 $mm^3 g^{-1}$, respectively. Figure 3 shows TEM images to show the morphology of the synthesized TiO_2 nanoparticles for the highest and lowest molar ratio (molar ratio = 50 for Figures 3(a) and 3(b) and molar ratio = 2 for Figures 3(c) and 3(d)). No difference in the particle shape was observed for the two samples with respect to the TiO_2 synthesis conditions. In addition, the synthesized particles were found to be aggregated and form many inter-aggregated pores. Hence, it is reasonable to hypothesize that the greater specific surface area and pore volume for the TiO_2 nanoparticles with higher molar ratio are likely due to the formation of more pores by the cohesion between aggregated particles. This hypothesis is supported by the result for the distribution of the pore sizes (Figure 4) for the synthesized TiO_2 samples according to the amount of water added. When a relatively small amount of water was added (molar ratio $\leq$ 10), the TiO_2 nanoparticles were found to mostly possess pores with the size of 2–5 nm; however, when molar ratio was greater than 20, the extra pores greater than 5 nm were observed to form. Moreover, for the samples with molar ratio of 20 and 50, it was observed that large quantity of extra pores with the size of 10 and 8 nm, respectively, formed as compared to those with low molar ratio. This result further confirmed that higher dosage of water led to the greater formation of the inter-aggregated pores due to the cohesion between TiO_2 nanoparticles. Consequently, larger specific surface area and higher pore volume for the synthesized TiO_2 nanoparticles with high molar ratio are thought to lead to better degradation efficiency for methylene blue [30–32].

3.2. Effect of Synthesis pH on Photocatalytic Activity of TiO_2. In order to investigate the effect of synthesis pH on photolysis efficiency of TiO_2 nanoparticles, the degradation rate of methylene blue by TiO_2 nanoparticles, which was synthesized under various pH levels of water, was examined and the results are presented in Figure 5 and Table 1. The amount of water added as a hydrolysis reagent was 5 mol (i.e., molar ratio of water and TTIP = 5), and the calcination temperature was fixed to 600°C. Similar with the results for molar ratio, the adsorption amount of methylene blue was greater than for the samples with high specific surface area (Tables 1 and 3).

Overall, the samples synthesized at low pH conditions exhibited greater photocatalytic activity than P25 (i.e., k = 0.536 h^{-1} for P25 and $k \geq 0.551\,h^{-1}$ for all samples

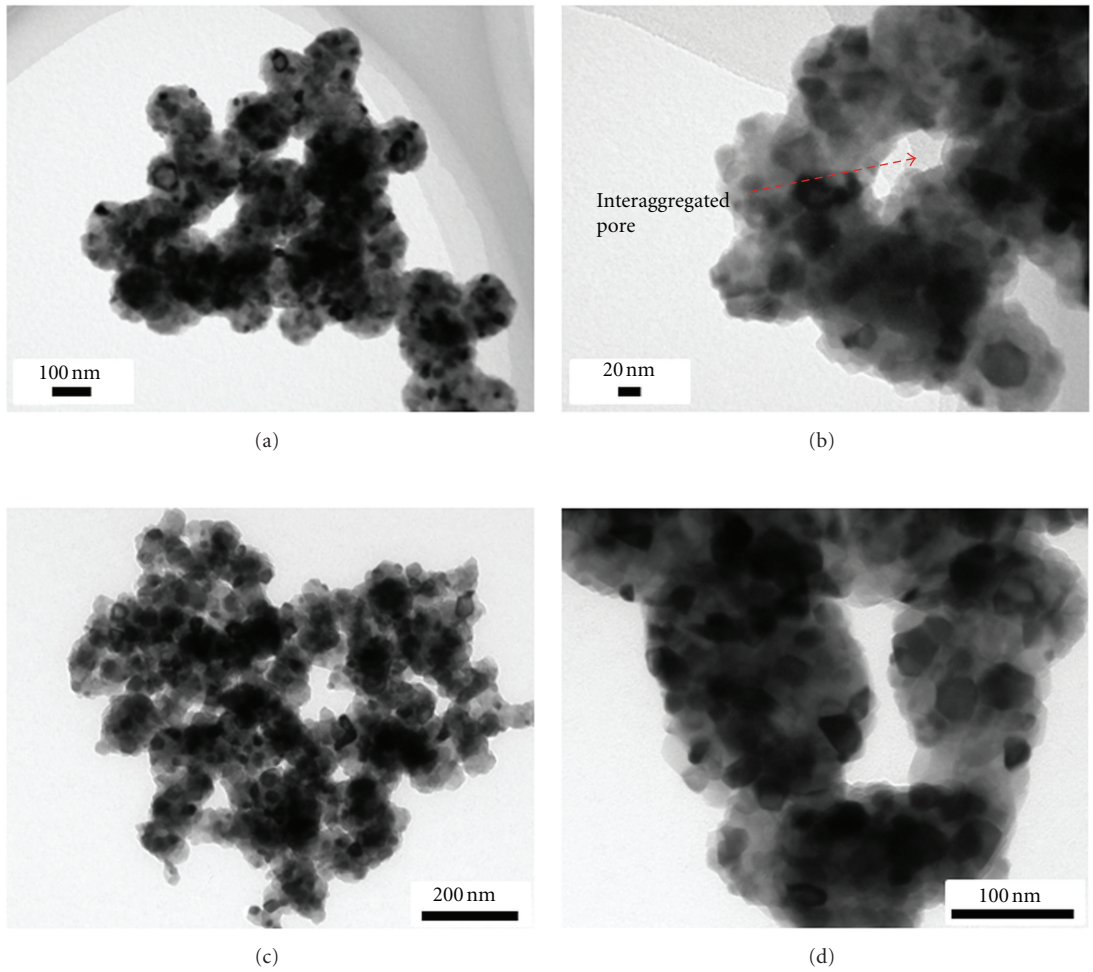

Figure 3: TEM images of TiO_2 nanoparticles synthesized with different molar ratios of water and TTIP: (a and b) 50 and (c and d) 2. The TiO_2 synthesis was carried out at pH 7 and at a calcination temperature of 600°C.

Table 3: Physicochemical properties of the TiO_2 nanoparticles synthesized with different pH conditions. The TiO_2 synthesis was carried out with a molar ratio (water and TTIP) of 5 and at a calcination temperature of 600°C.

pH	Phase content[a]	S_{BET}[b] ($m^2\,g^{-1}$)	Pore volume[b] ($mm^3\,g^{-1}$)	Crystalline size[c] (nm)
2.5	(A): 100	32.2	45	13.2
4	(A): 100	25.5	33	17.0
7	(A): 100	38.2	69	18.0
9	(A): 33.2	16.8	28	(A): 21.4
	(R): 66.8			(R): 23.0
11	(A): 10.3	46.3	58	(A): 22.1
	(R): 89.7			(R): 28.5

[a]A and R represent anatase and rutile, respectively.
[b]Value calculated from nitrogen adsorption isotherm.
[c]Value calculated using the Scherrer's equation [22].

synthesized) (Table 1). Especially, the TiO_2 sample synthesized at pH 2.5 showed the best photocatalytic activity (i.e., $k = 0.894\,h^{-1}$). The above results indicate that photocatalytic activity of synthesized TiO_2 nanoparticles is a function of the synthesis pH of water which was used as a hydrolysis reagent [33].

Figure 6 and Table 3 illustrate XRD patterns of TiO_2 samples synthesized under different pH conditions. Anatase phase was observed when hydrolysis reagent was acidic (pH ≤ 7), but as pH increased, crystalline phase of synthesized TiO_2 showed a transition to the rutile phase (pH ≥ 9), which is consistent with the results observed from a previous

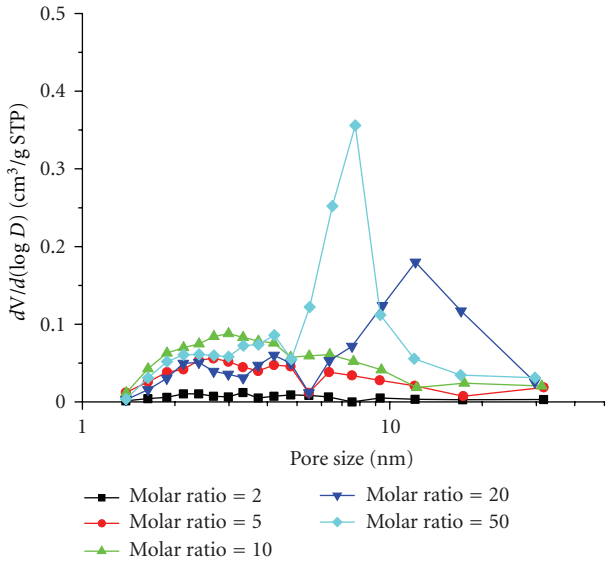

Figure 4: BJH pore size distributions for TiO_2 nanoparticles synthesized with different molar ratios of water and TTIP. The TiO_2 synthesis was carried out at pH 7 and at a calcination temperature of 600°C.

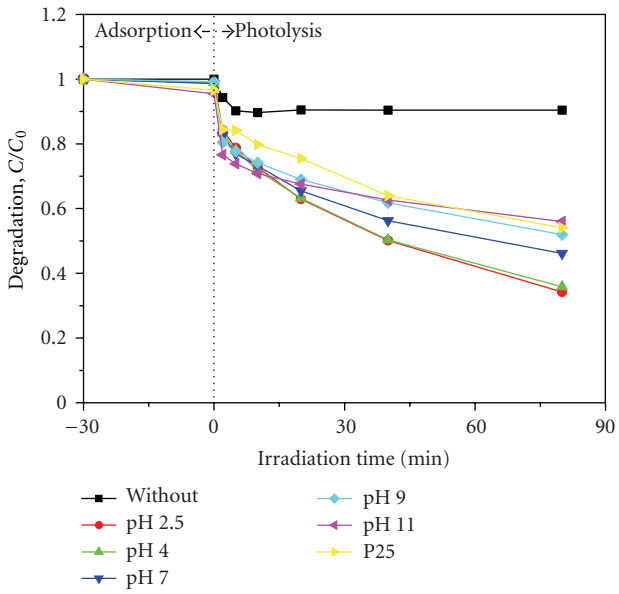

Figure 5: Photocatalytic degradation of methylene blue by TiO_2 nanoparticles synthesized at different pH conditions. The TiO_2 synthesis was carried out with a molar ratio (water and TTIP) of 5 and a calcination temperature of 600°C. The results from the experiments with P25 and without TiO_2 nanoparticles were also presented for comparison purpose.

study [29]. Specifically, an anatase phase was observed at pH 2.5, and the anatase peak increased up to pH 7 with maximum peak value (Figure 5); however, rutile peak started to be observed at pH 9, and the peak was more pronounced for the sample at pH 11.

The sizes of TiO_2 synthesized under different pH were observed to increase in accordance with increasing pH

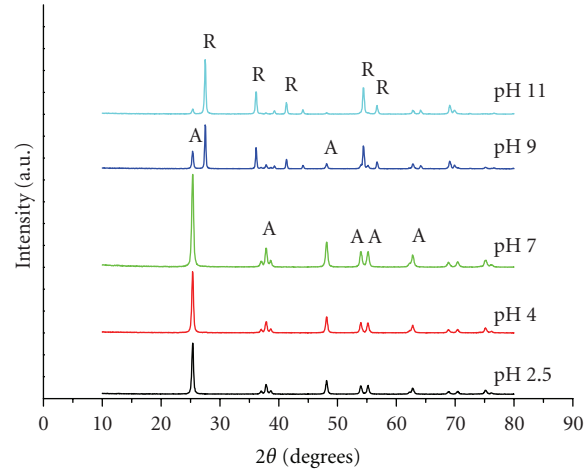

Figure 6: XRD patterns of TiO_2 nanoparticles synthesized at different pH conditions. The TiO_2 synthesis was carried out with a molar ratio (water and TTIP) of 5 and a calcination temperature of 600°C. A and R represent anatase and rutile, respectively.

(Table 3). It has been known that phase transition of TiO_2 led to the increase in crystallite size [34], which is consistent with our results. Specifically, as the synthesis pH increased, phase transition occurred in synthesized TiO_2 nanoparticles, and eventually crystallite size slightly increased. The results from both crystalline phase and crystallite size for synthesized TiO_2, suggest that photocatalytic activity of TiO_2 is expected to be maximized at pH 7 since anatase crystallinity was greatest at pH 7 with similar crystallite size as compared to that at other pH conditions [35–37]. However, samples synthesized at acidic conditions (i.e., pH 2 and 4) showed the best photocatalytic activity, implying that it was not enough to explain the result of photocatalytic performance only by the properties of crystallinity and crystallite size of TiO_2 nanoparticles.

Previously, some studies reported that the more OH groups existed on the surface of TiO_2, the greater photocatalytic activity appeared [38, 39]. Hence, the degree of OH groups existing on the surface of synthesized TiO_2 samples was also investigated using FT-IR spectra in this study. The FT-IR spectra of the nanocrystallite TiO_2 powders are shown in Figure 7. The broad peak appearing between 3200 and 3600 cm^{-1} is assigned to the stretching vibrations of the OH groups [40]. The peaks in the range of 1620–1630 cm^{-1} are attributed to the bending vibrations of the surface-adsorbed water molecules [41]. The main peak appearing in the range 650–700 cm^{-1} corresponds to Ti–O and Ti–O–Ti stretching vibrations [41, 42]. The FT-IR spectra of all samples showed the characteristic peaks of Ti–O and Ti–O–Ti stretching vibrations in the range of 650–700 cm^{-1}. However, the amount of adsorbed water molecules and hydroxyl groups was different between the samples synthesized at different pH conditions as evidenced by the intensity of the bands corresponding to the bending vibrations of surface-adsorbed molecules (1620–1630 cm^{-1}) and the stretching vibrations of the hydroxyl groups (3200–3600 cm^{-1}). Relatively huge difference in the FT-IR spectra was observed in the intensity

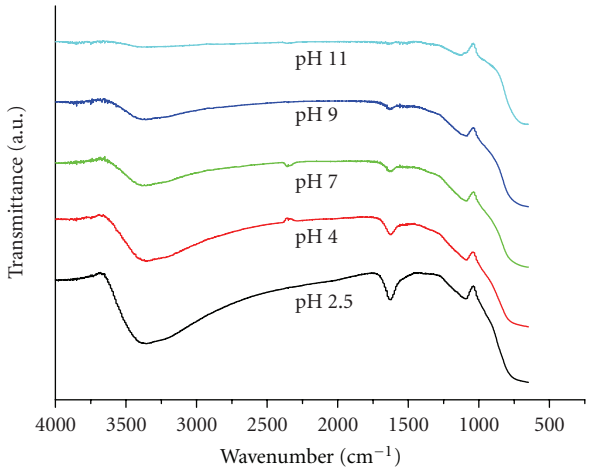

Figure 7: FT-IR spectra of TiO_2 nanoparticles synthesized at different pH conditions. The TiO_2 synthesis was carried out with a molar ratio (water and TTIP) of 5 and a calcination temperature of 600°C.

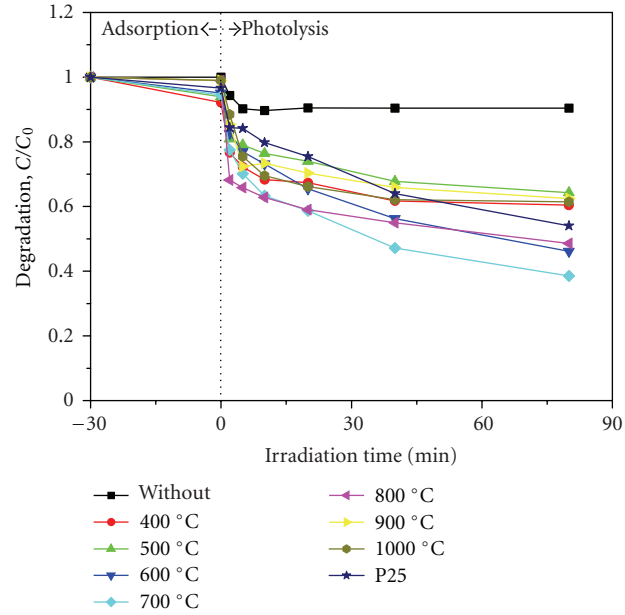

Figure 8: Photocatalytic degradation of methylene blue by TiO_2 nanoparticles synthesized with different calcination temperatures. The TiO_2 synthesis was carried out with a molar ratio (water and TTIP) of 5 and pH 7. The results from the experiments with P25 and noncalcined TiO_2 and without TiO_2 nanoparticles were also presented for comparison purpose.

of the peak appearing between 3200 and 3600 cm^{-1} assigned to the stretching vibrations of the hydroxyl group. Additionally, the sample synthesized under more acidic conditions was observed to possess larger amount of adsorbed water. The FT-IR results indicate that the amount of adsorbed water molecules and hydroxyl groups on the surface of TiO_2 nanoparticles is closely related to their photocatalytic activity. It has been previously reported that, during a sol-gel process under low pH condition, hydrolysis reaction is facilitated and condensation reaction is delayed [17].

Furthermore, it has been also reported that, under acidic conditions, positive charge of OR group partially increased to accelerate the hydrolysis reaction because OH group can easily attach on the surface of titanium ions in accordance with increasing repulsive force between positive charge of titanium ion and the OR group [17, 43, 44]. Consistent with the previous studies, our results also suggest that, under the low pH condition, the interaction between hydrogen and oxygen actively occurred during hydrolysis reaction, leading to the formation of water molecules adsorbed on the surface of the TiO_2 powder, and accordingly, the increasing concentration of hydroxyl group and water molecules on the surface of TiO_2. Therefore, the FT-IR (Figure 7) and methylene blue degradation experimental results (Figure 5 and Table 1) implied that photocatalytic activity of TiO_2 nanoparticles was enhanced under low synthesis pH conditions due to the presence of abundant hydroxyl groups and water molecules existing on the surface of TiO_2. Yu et al. [33] also observed the similar trend which was attributed to the improved acidity (i.e., the number of surface acid sites) of the samples synthesized at acidic pH conditions pH.

3.3. Effect of Calcination Temperature on Photocatalytic Activity of TiO_2. Figure 8 and Table 1 show methylene blue degradation efficiency by TiO_2 nanoparticles synthesized at pH 7 with a 5 mol addition of water (i.e., molar ratio of water and TTIP = 5) according to different calcination temperatures. For the reactors without TiO_2 particles, no degradation was observed above 5 min after UV irradiation. On the other hand, all calcined TiO_2 samples showed continuous methylene blue degradation. The efficiency increased up to 700°C (e.g., $k = 0.871\ h^{-1}$ for the sample calcined at 700°C) but decreased with calcination temperature above that point ($k < 0.871\ h^{-1}$ when calcination temperature > 700°C). A similar trend was also observed from several previous studies [45–47]. Additionally, the sample calcined at 1000°C only exhibited photocatalytic activity up to 20 min, and even after about 80 min the degree of activity was almost identical with that of the samples calcined at 500°C or below (Figure 8). The trend is likely due to relatively short reaction time (i.e., ca. 90 min) investigated in this study, which may not be enough to see the distinct difference between both samples (Figure 8) [24, 48, 49]. Another plausible explanation could be the combined effect of the degree of crystallinity which was improved with increasing temperature and the specific surface area which decreased with increasing calcination temperature (Table 4).

In order to understand the trend for the methylene blue degradation efficiency by TiO_2 nanoparticles with different calcination temperatures, crystalline structure and crystallite size of TiO_2 nanoparticles were investigated. Figure 9 and Table 4 show XRD patterns for TiO_2 nanoparticles calcined at different temperatures. Anatase peak started to appear at 400°C and increased up to 700°C. Rutile phase started to appear at 700°C, and the intensity increased from that point with almost no anatase phase at 900°C (i.e., anatase phase content = ~3.7 at 900°C) (Table 4). It was also observed

Table 4: Physicochemical properties of the TiO_2 nanoparticles synthesized with different calcination temperatures. The TiO_2 synthesis was carried out with a molar ratio (water and TTIP) of 5 and pH 7.

Temperature (°C)	Phase content[a]	S_{BET}[b] ($m^2\,g^{-1}$)	Pore volume[b] ($mm^3\,g^{-1}$)	Crystalline size[c] (nm)
400	(A): 100	83.3	85	9.6
500	(A): 100	40.1	55	13.7
600	(A): 100	38.2	69	18.0
700	(A): 92.4	33.1	46	(A): 28.5
	(R): 7.6			(R): 33.1
800	(A): 15.1	22.3	32	(A): 58.9
	(R): 84.9			(R): 94.1
900	(A): 3.7	19.5	30	(A): 77.2
	(R): 96.3			(R): 113
1000	(R): 100	16.1	26	138

[a]A and R represent anatase and rutile, respectively.
[b]Value calculated from nitrogen adsorption isotherm.
[c]Value calculated using the Scherrer's equation [22].

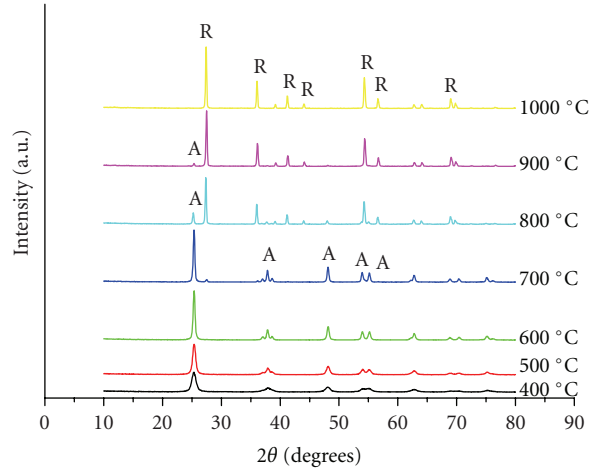

Figure 9: XRD patterns of TiO_2 nanoparticles synthesized with different calcination temperatures. The TiO_2 synthesis was carried out with a molar ratio (water and TTIP) of 5 and pH 7. A and R represent anatase and rutile, respectively.

that anatase phase was totally disappeared and transformed to rutile phase at 1000°C. This result is consistent with a previous study which reported that TiO_2 synthesized via a common sol-gel process showed phase transition at around 600°C or higher temperature [15]. Crystallite size of TiO_2 particles with different calcination temperatures is also presented in Table 4. Overall, crystallite size increased with increasing calcination temperature, showing substantial increase at the temperature range between 700 and 800°C. More specifically, the anatase crystallite size of the samples calcined at 700 and 800°C was determined to be 28.5 and 58.9 nm, respectively (Table 4). These results suggest that crystallite size and phase transition were much more influenced by calcination temperature as compared to the amount of water addition (i.e., molar ratio of water and TTIP) and pH among the variables adjusted in the process of TiO_2 synthesis investigated herein.

Specific surface area and pore volume of TiO_2 particles synthesized at different calcination temperatures are listed in Table 4. Specific surface area and pore volume of the sample with lowest calcination temperature (i.e., 400°C) were determined to be 83.3 $m^2\,g^{-1}$ and 85 $mm^3\,g^{-1}$, respectively. However, both specific surface area and pore volume gradually decreased with increasing calcination temperature, and the sample calcined at 1000°C showed the lowest values (S_{BET} = 16.1 $m^2\,g^{-1}$ and pore volume = 26 $mm^3\,g^{-1}$). These results are consistent with the finding from the previous study which reported the inverse relationship between crystallite size and specific surface area [23]. If specific surface area and pore volume of TiO_2 nanoparticles were dominant factors controlling the photocatalytic activity of TiO_2, the activity would have decreased with calcination temperature; however, the activity showed the maximum value at 700°C. The trend is likely attributed to the combined effect of anatase crystallinity which showed the highest intensity at 700°C (Figure 9) [13] and crystallite size which did not excessively increase up to 700°C (Table 4). Furthermore, the decreasing photocatalytic activity for the samples with a calcination temperature of 800°C or above could be explained by the decreased specific surface area and the subsequent reduction in the adsorption sites for the degradation reaction due to the decrease in anatase crystallinity and the excessive growth in crystallite size [31, 32].

4. Conclusions

In the present study, the degradation behavior of methylene blue by TiO_2 nanoparticles, which were synthesized under different synthesis conditions (i.e., molar ratio of water and TTIP, pH, and calcination temperature) in a sol-gel process, was investigated. The correlation between physical properties and photocatalytic activity of TiO_2 nanoparticles according to the different synthesis conditions is as follows.

(i) The amount of water added (i.e., molar ratio of water and TTIP), which was used as hydrolysis reagent, did not significantly influence the change in the crystallite size of TiO_2 nanoparticles; however, anatase

crystallinity slightly decreased for the TiO_2 synthesized with large molar ratio of water and TTIP (i.e., 50). The increasing molar ratio led to the enhanced photocatalytic activity of TiO_2 nanoparticles. The results were likely attributed to the increased specific surface area of TiO_2 nanoparticles synthesized with high molar ratio, which resulted from the relative increase in the size of the inter-aggregated pores of aggregated TiO_2 nanoparticles.

(ii) TiO_2 nanoparticles synthesized at acidic conditions (i.e., pH 2 and 4) showed the best photocatalytic activity. However, the results were not explained by the physical properties for the crystallinity and the crystallite size of TiO_2 nanoparticles but explained by the extent of active surface functional groups (e.g., hydroxyl group). Specifically, under low pH conditions, photocatalytic activity of TiO_2 nanoparticles was enhanced by the presence of abundant hydroxyl groups and water molecules existing on the surface of TiO_2.

(iii) Methylene blue degradation experiments revealed that the photocatalytic activity of TiO_2 nanoparticles was maximized at the calcination temperature of 700°C. However, specific surface area and pore volume of TiO_2 nanoparticles gradually decreased with increasing calcination temperature, indicating that those physical properties were not critical for controlling the photocatalytic activity of TiO_2 nanoparticles. The trend was likely due to the combined effect of the anatase crystallinity which showed the highest value at 700°C and the crystallite size which did not excessively increase up to 700°C.

The findings from this study indicate that physical properties of TiO_2 nanoparticles, which played an important role on photocatalytic activity of TiO_2, can be controlled by varying the synthesis conditions, such as amount of water addition (i.e., molar ratio of water and TTIP), pH, and calcination temperature.

Acknowledgments

This paper was supported by the Basic Research Project (12-530290) of the Korea Institute of Geoscience and Mineral Resources (KIGAM) and funded by the Ministry of Knowledge Economy of Korea.

References

[1] S. Boujday, F. Wünsch, P. Portes, J.-F. Bocquet, and C. C. Justin, "Photocatalytic and electronic properties of TiO_2 powders elaborated by sol-gel route and supercritical drying," *Solar Energy Materials and Solar Cells*, vol. 83, no. 4, pp. 421–433, 2004.

[2] H. Chen, C. Su, J. Chen, T. Yang, N. Hsu, and W. Li, "Preparation and characterization of pure rutile TiO_2 nanoparticles for photocatalytic study and thin films for dye-sensitized solar cells," *Journal of Nanomaterials*, vol. 2011, Article ID 869618, 8 pages, 2011.

[3] O. Legrini, E. Oliveros, and A. M. Braun, "Photochemical processes for water treatment," *Chemical Reviews*, vol. 93, no. 2, pp. 671–698, 1993.

[4] M. Srinivasan and T. White, "Degradation of methylene blue by three-dimensionally ordered macroporous titania," *Environmental Science and Technology*, vol. 41, no. 12, pp. 4405–4409, 2007.

[5] Q. Zhang, L. Gao, and J. Guo, "Effects of calcination on the photocatalytic properties of nanosized TiO_2 powders prepared by $TiCl_4$ hydrolysis," *Applied Catalysis B*, vol. 26, no. 3, pp. 207–215, 2000.

[6] J. Sin, S. Lam, A. R. Mohamed, and K. Lee, "Degrading endocrine disrupting chemicals from wastewater by TiO_2 photocatalysis: a review," *International Journal of Photoenergy*, vol. 2012, Article ID 185159, 23 pages, 2012.

[7] M. I. Litter, "Heterogeneous photocatalysis: transition metal ions in photocatalytic systems," *Applied Catalysis B*, vol. 23, no. 2-3, pp. 89–114, 1999.

[8] W. Li, C. Liu, Y. Zhou et al., "Enhanced photocatalytic activity in anatase/TiO_2(B) core-shell nanofiber," *Journal of Physical Chemistry C*, vol. 112, no. 51, pp. 20539–20545, 2008.

[9] S. Liu, J. Yu, and M. Jaroniec, "Anatase TiO_2 with dominant high-energy 001 facets: synthesis, properties, and applications," *Chemistry of Materials*, vol. 23, no. 18, pp. 4085–4093, 2011.

[10] S. Liu, J. Yu, and M. Jaroniec, "Tunable photocatalytic selectivity of hollow TiO_2 microspheres composed of anatase polyhedra with exposed 001 facets," *Journal of the American Chemical Society*, vol. 132, no. 34, pp. 11914–11916, 2010.

[11] J. Yu, H. Yu, B. Cheng, M. Zhou, and X. Zhao, "Enhanced photocatalytic activity of TiO_2 powder (P25) by hydrothermal treatment," *Journal of Molecular Catalysis A*, vol. 253, no. 1-2, pp. 112–118, 2006.

[12] A. Fujishima, T. N. Rao, and D. A. Tryk, "Titanium dioxide photocatalysis," *Journal of Photochemistry and Photobiology C*, vol. 1, no. 1, pp. 1–21, 2000.

[13] G. Tian, H. Fu, L. Jing, and C. Tian, "Synthesis and photocatalytic activity of stable nanocrystalline TiO_2 with high crystallinity and large surface area," *Journal of Hazardous Materials*, vol. 161, no. 2-3, pp. 1122–1130, 2009.

[14] B. B. Lakshmi, C. J. Patrissi, and C. R. Martin, "Sol-gel template synthesis of semiconductor oxide micro- and nanostructures," *Chemistry of Materials*, vol. 9, no. 11, pp. 2544–2550, 1997.

[15] J. Zhang, M. Li, Z. Feng, J. Chen, and C. Li, "UV raman spectroscopic study on TiO_2. I. Phase transformation at the surface and in the bulk," *The Journal of Physical Chemistry B*, vol. 110, no. 2, pp. 927–935, 2006.

[16] T. Cao, Y. Li, C. Wang, C. Shao, and Y. Liu, "One-step nonaqueous synthesis of pure phase TiO_2 nanocrystals from $TiCl_4$ in butanol and their photocatalytic properties," *Journal of Nanomaterials*, vol. 2011, Article ID 267415, 6 pages, 2011.

[17] J. P. Nikkanen, T. Kanerva, and T. Mäntylä, "The effect of acidity in low-temperature synthesis of titanium dioxide," *Journal of Crystal Growth*, vol. 304, no. 1, pp. 179–183, 2007.

[18] M. N. Chong, B. Jin, C. W. K. Chow, and C. Saint, "Recent developments in photocatalytic water treatment technology: a review," *Water Research*, vol. 44, no. 10, pp. 2997–3027, 2010.

[19] U. I. Gaya and A. H. Abdullah, "Heterogeneous photocatalytic degradation of organic contaminants over titanium dioxide: a review of fundamentals, progress and problems," *Journal of Photochemistry and Photobiology C*, vol. 9, no. 1, pp. 1–12, 2008.

[20] J. Yu, G. Wang, B. Cheng, and M. Zhou, "Effects of hydrothermal temperature and time on the photocatalytic activity and microstructures of bimodal mesoporous TiO_2 powders," *Applied Catalysis B*, vol. 69, no. 3-4, pp. 171–180, 2007.

[21] Y. Li, X. Li, J. Li, and J. Yin, "Photocatalytic degradation of methyl orange by TiO_2-coated activated carbon and kinetic study," *Water Research*, vol. 40, no. 6, pp. 1119–1126, 2006.

[22] D. S. Kim, S. J. Han, and S. Y. Kwak, "Synthesis and photocatalytic activity of mesoporous TiO_2 with the surface area, crystallite size, and pore size," *Journal of Colloid and Interface Science*, vol. 316, no. 1, pp. 85–91, 2007.

[23] G. Oskam, A. Nellore, R. L. Penn, and P. C. Searson, "The growth kinetics of TiO_2 nanoparticles from titanium(IV) alkoxide at high water/titanium ratio," *Journal of Physical Chemistry B*, vol. 107, no. 8, pp. 1734–1738, 2003.

[24] H. Kim, S. Lee, Y. Han, and J. Park, "Preparation of dip-coated TiO_2 photocatalyst on ceramic foam pellets," *Journal of Materials Science*, vol. 41, no. 18, pp. 6150–6153, 2006.

[25] S. Brunauer, P. H. Emmett, and E. Teller, "Adsorption of gases in multimolecular layers," *Journal of the American Chemical Society*, vol. 60, no. 2, pp. 309–319, 1938.

[26] J. Yu, S. Liu, and H. Yu, "Microstructures and photoactivity of mesoporous anatase hollow microspheres fabricated by fluoride-mediated self-transformation," *Journal of Catalysis*, vol. 249, no. 1, pp. 59–66, 2007.

[27] E. P. Barrett, L. G. Joyner, and P. P. Halenda, "The determination of pore volume and area distributions in porous substances. I. Computations from nitrogen isotherms," *Journal of the American Chemical Society*, vol. 73, no. 1, pp. 373–380, 1951.

[28] J. Yu, J. C. Yu, M. K. P. Leung et al., "Effects of acidic and basic hydrolysis catalysts on the photocatalytic activity and microstructures of bimodal mesoporous titania," *Journal of Catalysis*, vol. 217, no. 1, pp. 69–78, 2003.

[29] B. Li, X. Wang, M. Yan, and L. Li, "Preparation and characterization of nano-TiO_2 powder," *Materials Chemistry and Physics*, vol. 78, no. 1, pp. 184–188, 2002.

[30] Y. Li, N. H. Lee, E. G. Lee, J. S. Song, and S. J. Kim, "The characterization and photocatalytic properties of mesoporous rutile TiO_2 powder synthesized through self-assembly of nano crystals," *Chemical Physics Letters*, vol. 389, no. 1–3, pp. 124–128, 2004.

[31] R. Tan, Y. He, Y. Zhu, B. Xu, and L. Cao, "Hydrothermal preparation of mesoporous TiO_2 powder from $Ti(So_4)_2$ with poly(ethylene glycol) as template," *Journal of Materials Science*, vol. 38, no. 19, pp. 3973–3978, 2003.

[32] T. Peng, D. Zhao, K. Dai, W. Shi, and K. Hirao, "Synthesis of titanium dioxide nanoparticles with mesoporous anatase wall and high photocatalytic activity," *Journal of Physical Chemistry B*, vol. 109, no. 11, pp. 4947–4952, 2005.

[33] J. Yu, Y. Su, B. Cheng, and M. Zhou, "Effects of pH on the microstructures and photocatalytic activity of mesoporous nanocrystalline titania powders prepared via hydrothermal method," *Journal of Molecular Catalysis A*, vol. 258, no. 1-2, pp. 104–112, 2006.

[34] S. Mahshid, M. Askari, and M. S. Ghamsari, "Synthesis of TiO_2 nanoparticles by hydrolysis and peptization of titanium isopropoxide solution," *Journal of Materials Processing Technology*, vol. 189, no. 1-3, pp. 296–300, 2007.

[35] V. Puddu, H. Choi, D. D. Dionysiou, and G. L. Puma, "TiO_2 photocatalyst for indoor air remediation: influence of crystallinity, crystal phase, and UV radiation intensity on trichloroethylene degradation," *Applied Catalysis B*, vol. 94, no. 3-4, pp. 211–218, 2010.

[36] X. Y. Chuan, M. Hirano, and M. Inagaki, "Preparation and photocatalytic performance of anatase-mounted natural porous silica, pumice, by hydrolysis under hydrothermal conditions," *Applied Catalysis B*, vol. 51, no. 4, pp. 255–260, 2004.

[37] Y. V. Kolen'ko, B. R. Churagulov, M. Kunst, L. Mazerolles, and C. Colbeau-Justin, "Photocatalytic properties of titania powders prepared by hydrothermal method," *Applied Catalysis B*, vol. 54, no. 1, pp. 51–58, 2004.

[38] A. Sclafani, L. Palmisano, and M. Schiavello, "Influence of the preparation methods of titanium dioxide on the photocatalytic degradation of phenol in aqueous dispersion," *The Journal of Physical Chemistry*, vol. 94, no. 2, pp. 829–835, 1990.

[39] S. J. Kim, H. G. Lee, S. J. Kim, J. K. Lee, and E. G. Lee, "Photoredox properties of ultrafine rutile TiO_2 acicular powder in aqueous 4-chlorophenol, Cu-EDTA and Pb-EDTA solutions," *Applied Catalysis A*, vol. 242, no. 1, pp. 89–99, 2003.

[40] X. Zhang, F. Zhang, and K. Y. Chan, "Synthesis of titania-silica mixed oxide mesoporous materials, characterization and photocatalytic properties," *Applied Catalysis A*, vol. 284, no. 1-2, pp. 193–198, 2005.

[41] Z. Ding, G. Q. Lu, and P. F. Greenfield, "Role of the crystallite phase of TiO_2 in heterogeneous photocatalysis for phenol oxidation in water," *Journal of Physical Chemistry B*, vol. 104, no. 19, pp. 4815–4820, 2000.

[42] L. Q. Jing, H. G. Fu, B. Q. Wang et al., "Effects of Sn dopant on the photoinduced charge property and photocatalytic activity of TiO_2 nanoparticles," *Applied Catalysis B*, vol. 62, no. 3-4, pp. 282–291, 2006.

[43] M. Gopal, W. J. Moberly Chan, and L. C. De Jonghe, "Room temperature synthesis of crystalline metal oxides," *Journal of Materials Science*, vol. 32, no. 22, pp. 6001–6008, 1997.

[44] P. Bonamali, S. Maheshwar, and N. Gyoichi, "Preparation and characterization of TiO_2/Fe_2O_3 binary mixed oxides and its photocatalytic properties," *Materials Chemistry and Physics*, vol. 59, no. 3, pp. 254–261, 1999.

[45] K. Lv, Q. Xiang, and J. Yu, "Effect of calcination temperature on morphology and photocatalytic activity of anatase TiO_2 nanosheets with exposed 0 0 1 facets," *Applied Catalysis B*, vol. 104, no. 3-4, pp. 275–281, 2011.

[46] J. Yu and B. Wang, "Effect of calcination temperature on morphology and photoelectrochemical properties of anodized titanium dioxide nanotube arrays," *Applied Catalysis B*, vol. 94, no. 3-4, pp. 295–302, 2010.

[47] J. G. Yu, H. G. Yu, B. Cheng, X. J. Zhao, J. C. Yu, and W. K. Ho, "The effect of calcination temperature on the surface microstructure and photocatalytic activity of TiO_2 thin films prepared by liquid phase deposition," *Journal of Physical Chemistry B*, vol. 107, no. 50, pp. 13871–13879, 2003.

[48] C. Wen, Y. J. Zhu, T. Kanbara, H. Z. Zhu, and C. F. Xiao, "Effects of I and F codoped TiO_2on the photocatalytic degradation of methylene blue," *Desalination*, vol. 249, no. 2, pp. 621–625, 2009.

[49] H. Le, L. Linh, S. Chin, and J. Jurng, "Photocatalytic degradation of methylene blue by a combination of TiO_2-anatase and coconut shell activated carbon," *Powder Technology*, vol. 225, pp. 167–175, 2012.